Pre-print Version - Article Published in Computers and Electrical Engineering 101 (2022) 108105
https://doi.org/10.1016/j.compeleceng.2022.108105

A deep learning approach for brain tumor classification using MRI images

Muhammad Aamir [a,*], Ziaur Rahman [a,*], Zaheer Ahmed Dayo [a], Waheed Ahmed Abro [b], M. Irfan Uddin [c], Inayat Khan [d], Ali Shariq Imran [e], Zafar Ali [b], Muhammad Ishfaq [a], Yurong Guan [a], Zhihua Hu [a]

[a] Department of Computer Science, Huanggang Normal University, Huanggang 438000, China
[b] School of Computer Science and Engineering, Southeast University, Nanjing 211189, China
[c] Institute of Computing, Kohat University of Science and Technology, Kohat 26000, Pakistan
[d] Department of Computer Science, University of Buner, Buner 19290, Pakistan
[e] Department of Computer Science, Norwegian University of Science and Technology, Gjøvik 2802, Norway

ARTICLE INFO

Keywords:
Healthcare
Deep learning features
Feature fusion
Illumination boost
Non-linear stretching
Localization
Refinement
MRI
Brain tumor classification
CAD

ABSTRACT

Brain tumors can be fatal if not detected early enough. Manually diagnosing brain tumors requires the radiologist's experience and expertise, which may not always be available. Furthermore, manual processes are inefficient, prone to errors, and time-taking. Therefore, an effective solution is required to ensure an accurate diagnosis. To this end, we propose an automated technique for detecting brain tumors using magnetic resonance imaging (MRI). First, brain MRI images are pre-processed to enhance visual quality. Second, we apply two different pre-trained deep learning models to extract powerful features from images. The resulting feature vectors are then combined to form a hybrid feature vector using the partial least squares (PLS) method. Third, the top tumor locations are revealed via agglomerative clustering. Finally, these proposals are aligned to a predetermined size and then relayed to the head network for classification. Compared to existing approaches, the proposed method achieved a classification accuracy of 98.95%.

1. Introduction

In today's world, medical specialists receive a vast amount of varying data. Their capacity for analyzing, collecting, and processing such large amounts of data is restricted. This makes them prone to weariness, impairing their ability to help patients control their health. In healthcare, 90% of data comprises images, which must be processed to create appropriate treatment plans and other uses. As a result, demand for medical image analysis is expanding, creating enormous prospects for developing innovative IT-based healthcare solutions [1]. Adopting these IT-based solutions enhances the diagnostic process for patients, i.e., increases diagnostic accuracy, decreases diagnostic time, and assists medical professionals and hospitals optimize their processes and operations. The brain is one of the most crucial and complex organs in the human body, processing billions of cells. It is the central nervous system component that regulates the operation of all other organs in the human body. However, uncontrolled, aberrant cell growth results in the formation of a tumor and impair the cell's activity [2]. Tumors vary in size, shape, and type and can grow in different locations across the brain. They

☆ This paper is for special section VSI-igdn. Reviews were processed by Guest Editor Dr. Hamid Reza Boveiri and recommended for publication.
* Corresponding authors at: Mr. Muhammad Aamir and Ziaur Rahman, Huanggang Normal University, China.
E-mail addresses: aamirshaikh86@hotmail.com (M. Aamir), ziaurrahman167@yahoo.com (Z. Rahman).

can be classed as cancerous or non-cancerous, high-grade or low-grade, malignant, pituitary, or benign [3].

Numerous medical imaging techniques are developed to obtain images for diagnosing various diseases. X-rays, ultrasonic imaging (UI), positron emission tomography (PET), computed tomography (CT), magnetic resonance spectroscopy (MRS), single-photon emission computed tomography (SPECT), and MRI are the most often used technologies [4]. These images aid the medical specialist in examining and obtaining thorough information about the various human body components. It also aids in disease diagnosis and therapy planning. However, MRI is the preferred and most valuable technique due to its ability to produce high-resolution images with precise information about the human body structure. For all tumor classes, such as Meningioma, Glioma, and Pituitary, MRI delivers a robust appearance. Further, MRI is also one of the most widely used and accurate medical imaging modalities for classifying brain tumors [5].

Brain tumor classification is significant and can save patient's lives. An accurate and timely diagnosis of a brain tumor is critical for the patient's treatment plan [6]. However, tumor classification is a complex and challenging challenge. Over the last few years, practitioners have put significant time and effort into making substantial advancements in classifying tumors in brain MRI images. Numerous strategies for achieving robust classification performance have been introduced [7]. Most brain tumor classification frameworks are still in infancy in their experimental findings. Because many factors, such as poor image quality, a lack of training data, low-quality image features, poor tumor localization, and others, might impact the brain tumor classification process.

As a result, developing a system capable of achieving state-of-the-art classification performance while simultaneously enhancing the factors mentioned above is challenging. Therefore, meticulous research to establish an advanced classifier is always active and critical. Thus, this paper presents the study from the perspective of brain tumor classification to provide researchers, academics, and practitioners with informative results. The proposed method can significantly increase the quality of computer-aided diagnosis (CAD), reduce the workload of medical specialists, and contribute to further alleviating the medical resource imbalance and contradictions between doctors and patients. It is vital to study the technical challenges surrounding the classification of brain tumors in medical imaging. This paper attempted to make improvements in the four aspects, and the following are the most significant contributions of this study:

- To improve the visual appearance of MRI images acquired using a variety of imaging modalities, non-linear stretching, and logarithmic scaling functions are applied.
- To use transfer learning to acquire more discriminative characteristics with adequate information.
- To provide a robust technique for tumor localization in MRI images using agglomerative clustering.
- To propose a high-accuracy classifier for classifying brain tumors using MRI images.

2. Related work

Brain tumors are one of the most deadly types of cancer in people of all ages. Their classification provides a substantial difficulty for radiologists involved in health monitoring and automated diagnosis. Numerous methods for brain tumor classification (BTC) based on machine learning have been recently reported in various research to assist radiologists in performing more accurate diagnostic analyses [8–20]. Machine learning has been incorporated into newly induced BTC methods which significantly impacts disease diagnosis performance and classification accuracy. Moreover, it enables neurologists to rapidly examine brain MRI images, enhance decision-making, and design an effective treatment plan. Due to their robust classification performance, machine learning-based BTC algorithms are gaining prominence. There are two types of machine learning-based BTC techniques: traditional machine learning-based and deep learning-based. Both groups undergo a series of processes to classify tumours in MRI images, including pre-processing, i.e., MRI image visual enhancement, localization, feature extraction, and classification. However, this is not always true for the BTC methods based on deep learning. These stages are mutually responsible for achieving superior classification performance. The primary goal of this study is to achieve a high level of classification accuracy by carefully examining each step involved in brain tumor classification. The following sections address previous works and research efforts to classify brain tumors using MRI images.

Cheng et al. suggested a model for improving the classification performance of brain tumors through tumor region augmentation and partitioning. They retrieved various features to evaluate their model's performance, including a bag-of-words (BOW), an intensity histogram, and a gray level co-occurrence matrix (GLCM). The support vector machine (SVM) is used to classify features and achieved an accuracy of 91.28% on a readily available Figshare dataset (https: /figshare.com/articles/braintumor dataset/1512427) of 3064 brain MRI images [8]. Ismael et al. developed a neural network-based model for brain tumor classification using the Figshare dataset based on two-dimensional discrete wavelet transform (2D-DWT) and 2D Gabor filter features [9]. Combining these statistical features improved classification performance and resulted in a 91.9%. Tahir et al. developed a model for classifying brain tumors based on MRI scans [10]. This model extracted 2D-DWT utilizing Daubechies wavelets base features to improve classification efficiency. SVM is used to ensure classification accuracy; the model achieved an accuracy of 86% on a Figshare dataset repository of 3064 brain MRI images.

Paul et al. proposed a brain tumor classification algorithm based on deep learning [11]. This approach enhanced classification accuracy using a convolutional neural network (CNN). On brain tumor Figshare imaging collection, the model achieved a 5-fold cross-validation accuracy of 90.26%. The model revealed that decreasing the size of an image can improve training performance and aid doctors during the patient treatment process. Afshar et al. developed a capsule network (CapsNet) model to effectively categorize brain tumors using the Figshare dataset [12]. The suggested network enhances classification accuracy by using the spatial relationships between the tumor and its surrounding tissues, which is a weakness of earlier CNN-based classification models [11,16,17]. The approach improves classification accuracy by using tumor-associated tissues as additional input. This model surpasses

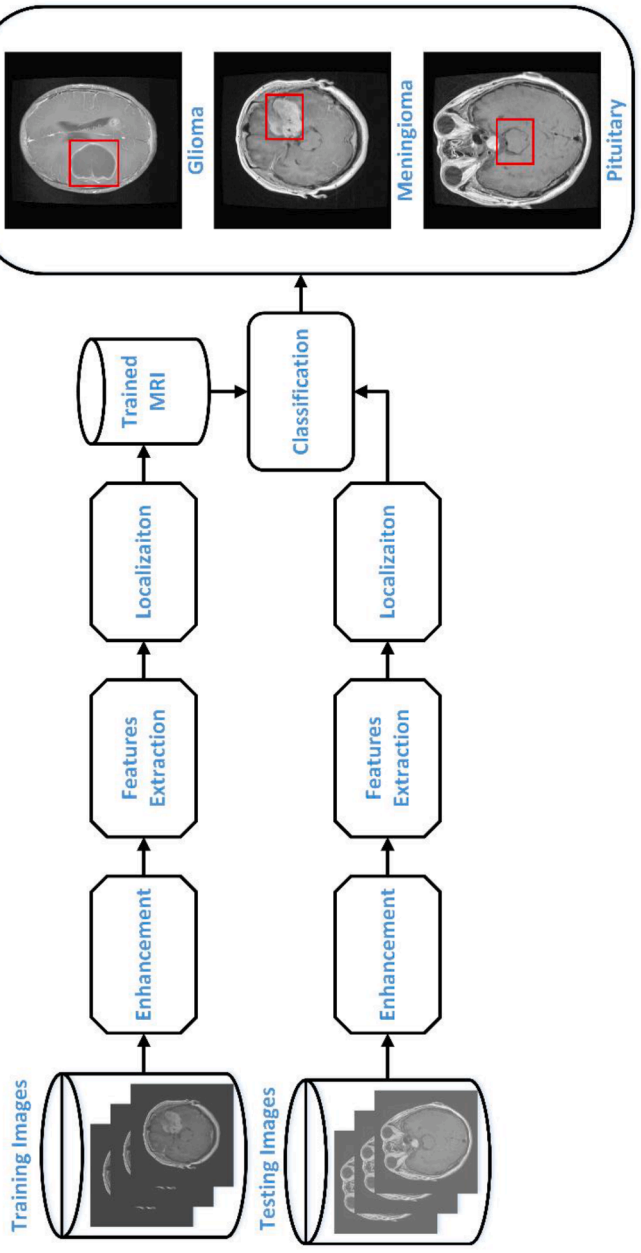

Fig. 1. Block diagram of the proposed model.

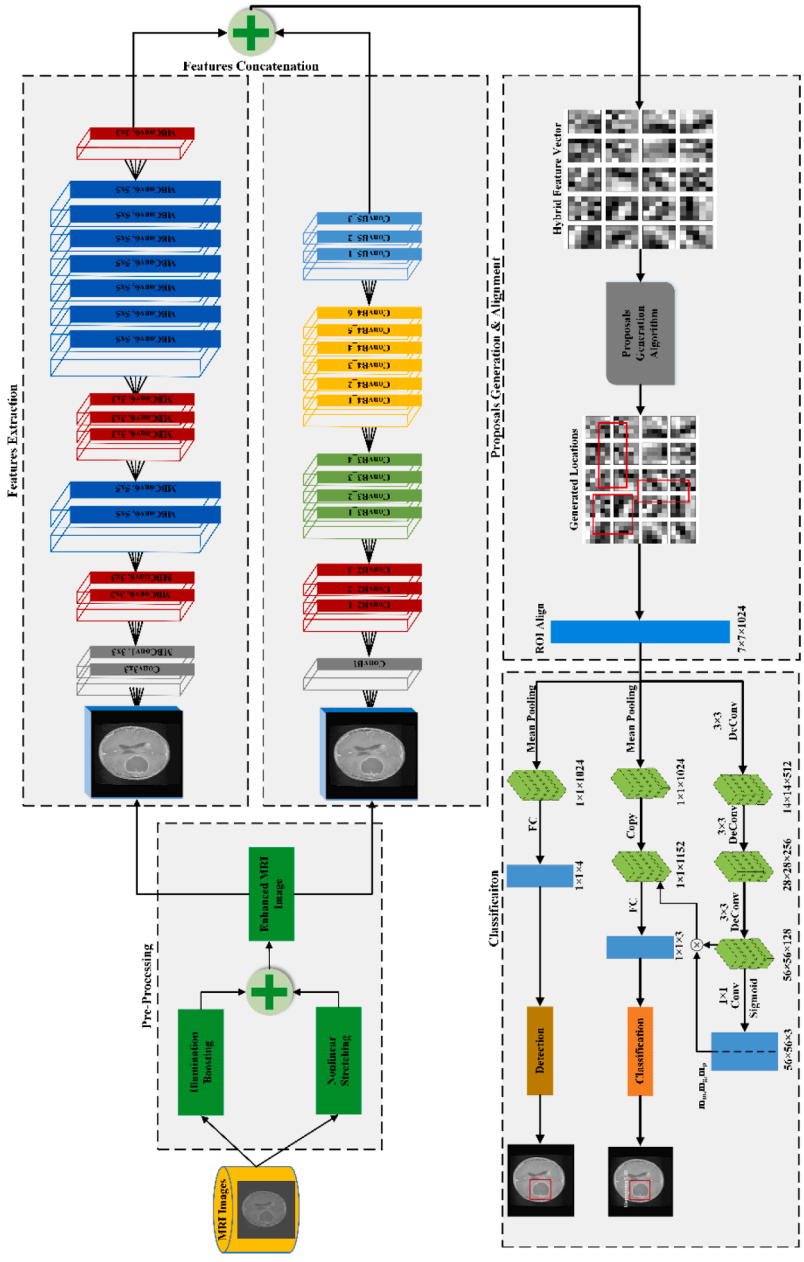

Fig. 2. The overall structural design of the proposed model The following are the significant steps involved in tumor classification:.

competitors [10,16,17] and achieves an accuracy of 86.56% with segmentation and 72.13% without segmentation, respectively.

Furthermore, Afshar et al. presented a modified CapsNet for brain tumor classification, which solves the drawbacks of CNN [13]. Unlike CNN, their model is resilient to input modifications such as rotation and affine transformation and requires less training data. This model outperformed competitors with a classification accuracy of 90.89% on Figshare imagery. Zhou et al. made a similar effort to increase classification accuracy using a holistic approach [14]. The method extracted information from axial slices in images and classified them using recurrent neural automated region segmentation. The model's excellent accuracy of 92.13% on Fighsare MRI images proves its usefulness. Pashaei et al. created a CNN-based algorithm for classifying brain tumors [15]. This method collects features from Figshare MRI images using a CNN and then classifies them using a kernel extreme learning machines (KELM) network. The experimental results indicate that this combined mechanism of CNN and KELM achieves a high level of accuracy, 93.68% when compared to other conventional machine learning classifiers such as radial basis function neural network (RBFNN), k-nearest neighbors (KNN), and SVM.

Abiwinanda et al. developed a model for brain tumor classification using CNN [16]. They generated seven distinct CNN variations without segmentation. Compared to earlier models, the second variant of their model obtains the highest training and testing accuracies of 98.51% and 84.19% on the Fighsare brain MRI dataset, respectively. Navid et al. provide another multi-class model for brain tumor classification based on a deep neural network [17]. The algorithm extracts information and learns the structure of Fighsare images using data augmentation approaches to pre-train a neural network as a discriminator in a generative adversarial network (GAN). The augmentation strategies prevent the network from becoming over-trained. The network's fully connected (FC) layers have been replaced to differentiate the tumor classes, and the model has been trained to function as a classifier. The model is assessed using five-fold cross-validation and achieves an accuracy of 95.6% on random splits and 93.01% on inserted splits.

Another study that investigated how genetic algorithms could increase the accuracy of CNN used to classify brain tumors was proposed by Anaraki et al. [18]. To improve the performance of their work, they modified the CNN architecture using a genetic algorithm. They achieved a maximum accuracy of 94.2% using the Fighshare dataset. Besides, to increase the efficacy of tumor classification, Ayadi et al. presented a deep CNN with many layers for brain tumor classification [19]. Three datasets, i.e., Figshare, Radiopaedia, and repository of molecular brain neoplasia data (REMBRANDT), evaluated the proposed model's efficacy. Their model demonstrated impressive performance and required significantly less pre-processing than previous approaches. Deepak et al. used transfer learning to increase the accuracy of three-class brain tumor classification [20]. Their model achieved a classification accuracy of 97.1% on MRI images gathered from Figshare, outperforming other systems that rely on a small number of training instances. The model also provided an analysis of misclassification.

The above analysis demonstrates that the presented research methodologies and models have shortcomings. To address these limitations, this work proposes to create innovative improvements in the following areas: addressing the problem of limited visibility in MRI images, low-quality features, a large number of object (tumor) locations or proposals, and a small dataset for improved classification performance.

3. Proposed method

The present paper aims to design an efficient and effective model for medical image analysis for detecting and classifying brain tumors using low-quality MRI images. The block diagram of the proposed model is presented in Fig. 1. The proposed method can extract robust features from MRI images, locate and classify tumors, and may serve as a helpful supplement to existing brain tumor classification methods. Radiologists stand to benefit from this applied research study in obtaining a second opinion that will aid them in determining the intensity, diameter, location, and kind of tumor. Early detection of brain tumors enables professionals to develop more effective treatment programs that result in healthier outcomes for the patient [21]. The proposed brain tumor classifier's framework is depicted in Fig. 2. Each patient's three MRI views were independently supplied into the network.

3.1. Enhancement

By studying medical images, a disease (brain tumor) can be identified for early treatment by specialists. However, low image visibility is a substantial impediment to effective disease diagnosis. The images created are complex and available to clinicians in various visual appearances, including high or low intensities, non-uniform, underexposed, overexposed, and noisy regions. Poor image quality considerably reduces the performance of the disease diagnostic procedure. This highlights the critical necessity to enhance contrast and maintain brightness in low-quality MRI pictures before efficiently executing tasks such as segmentation, detection, and classification on MRI images. It is exceedingly difficult to extract valuable structural information from images of poor visual quality.

Numerous contrast enhancement methods have been developed and deployed to various machine learning applications; improved visualization helps machine learning algorithms extract more useful characteristics from imagery [21]. This paper increased classification performance by providing a more transparent and visible input image to our network. An illumination boost approach is devised to improve the contrast of low-quality MRI images. The non-stretching method enhances the textural information in the MRI images. The following details are included:

3.1.1. Illumination boost

It begins by applying a logarithmic scale function to the input image. This function assesses the transformation that the human visual system's retina undergoes [22]. Also, it can boost low- and mid-intensity levels while protecting high-intensity levels from severe escalation. The following equation is used to compute this function.

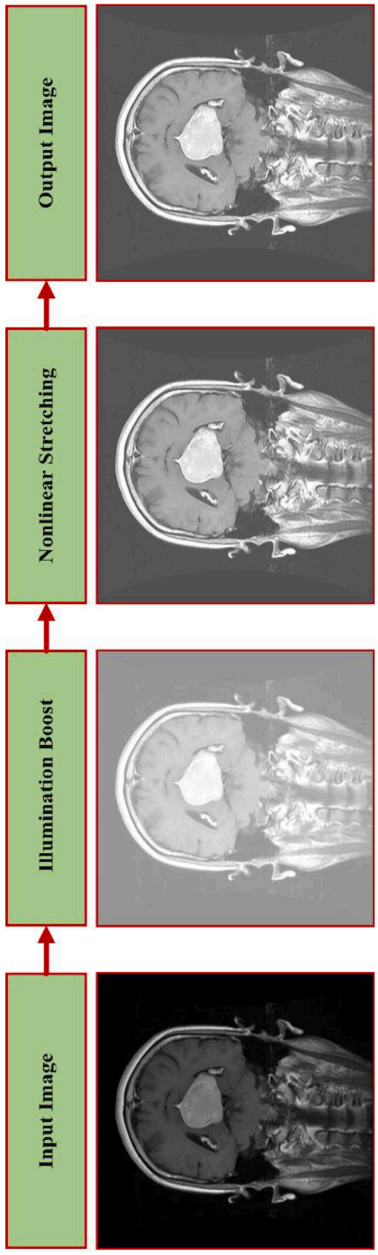

Fig. 3. Diagram depicting the process of image enhancement.

$$img_1 = \frac{\max(I)}{\log(max(I)+1)} \times \log(I+1) \tag{1}$$

Where, I denotes the low contrast brain MRI image, img_1 denotes the image produced by the logarithmic scaling function, and * denotes the multiplication operator. Following that, the input image I is processed again with a simple exponential function to alter the local contrast and attenuate the input image's high intensities. The following equation is used to calculate this function [22]:

$$img_2 = 1 - e^{-I} \tag{2}$$

where, img_2 is the image produced by the exponential function applied. Following that, images img_1 and img_2 are merged using an appropriate logarithmic image processing (LIP) model. As a result, many LIP models exist to combine the properties of two images. However, when evaluated on various brain MRI images, one of the LIP models outlined in [22] can produce encouraging results. The LIP model that was utilized can be computed as follows:

$$img_3 = \frac{img_1 + img_2}{\lambda + (img_1 \times img_2)} \tag{3}$$

where, λ is a scalar quantity that controls the enhancement process and is used to prevent the development of improper pixel values. At this time, image img_3 possesses the properties of both img_1 andimg_2. Despite this, the image's brightness is low, necessitating further augmentation to reveal most of the hidden image information. A modified cumulative distribution function of hyperbolic secant distribution (CDF-HSD) increases the overall brightness. The standard HSD function is a well-known function in probability and statistics. The CDF function utilized in this method is a type of S-curve function that can adjust the brightness and contrast. The standard CDF-HSD is calculated as follows:

$$img_4 = erf\left(\lambda \times \arctan\left(e^{img_3}\right) - 0.5 \times img_3\right) \tag{4}$$

where, img_4 is the image produced by the CDF-HSD equation.

The changes made significantly improved the function's processing efficiency in terms of brightness enhancement. First, the error function (erf) is introduced to the CDF-HSD equation to boost the curved transformation, which improves the brightness of the dark image sections. Furthermore, the value λ regulates the amount of enhancement, resulting in more brightness in the output image.

Moreover, subtracting the value $0.5 \times img_3$ helped normalize the image's tonality, making it more comparable to the observed scenario. Despite this, image img_4's pixel distribution is confined to a small dynamic range, giving the image a white appearance. As a result, the pixel values are linearly scaled to fit inside the required range using a normalization function. The following equation is used to calculate the normalization function [22]:

$$img_5 = \frac{img_4 - \min(img_4)}{\max(img_4) - \min(img_4)} \tag{5}$$

where, img_5 is the boost illumination algorithm's final output.

3.1.2. Non-linear stretching

Non-linear stretching functions increase the amount of textural information in an image while decreasing the amount of local brightness. The task is mathematically defined as,

$$N_s = signimg_5 \left(\frac{|img_5|}{\max(img_5)}\right)^{\alpha} .\max(|img_5|) \tag{6}$$

The stretching effect is produced by Eq. (6); the smaller the value of α, the greater the stretching. This parameter α controls the stretching effect of images. A smaller value of α, for example, achieves maximum brightness stretching, but a higher value of αrenders visual contrast. On the other hand, the authors assigned an ideal value to each image. Finally, as seen in Fig. 3, the improved image can be recreated.

3.2. Features extraction

The extraction of features is a critical step in image classification. These features help identify an object characterized by its name, size, form, and color. Any classifier's efficiency and accuracy are determined by the strength and efficacy of the retrieved features. To achieve high-quality classification results, we used two separate pre-trained deep learning models, i.e., EfficientNet and ResNet50, to extract features from images. Combining the resulting feature vectors yields a hybrid feature vector. However, this hybrid feature vector includes substantially more rich information about the image than a single feature vector and significantly improves a subsequent job's performance. The PLS-based fusion approach is utilized to merge many features into a single vector [23]. Assume that $R_v(1)$has a size of $X_1 \times K$ and $E_v(2)$ has a dimension of $X_2 \times K$are the two feature vectors generated by pre-trained models. Assume that $F_v(j)$ is the fused feature vector of a dimension of $X_3 \times K$. Additionally, we suppose that $\overrightarrow{U}$and $\overrightarrow{V}$ are the central variables of the vectors $R_v$andE_v, with a mean of zero.

Let $\delta_{uv} = \overrightarrow{U}\overrightarrow{V}$and $\delta_{uv} = \delta_{UV}^{T}\left(\left(\frac{1}{n}-1\right)\delta_{uv}\right)$ is set covariance among vectors $\overrightarrow{U}$ and $\overrightarrow{V}$. This PLS-based fusion preserves associated

characteristics while attempting to minimize prediction numbers. The mechanism of breakdown between $\overrightarrow{U}$ and $\overrightarrow{V}$is mathematically explained as follows:

$$\overrightarrow{U} = \sum_{i=}^{d} R_{V_i}(1i)^T = E \tag{7}$$

$$\overrightarrow{V} = \sum_{i=}^{d} E_{V_i}(2i)^T = F \tag{8}$$

when PLS is used, the following pair of directions between $u_i$and $v_i$can be determined:

$$\{u_i; v_i\} = \arg \max_{u^T u=V^T v=1} Cov\left(\overrightarrow{U}^T u, \overrightarrow{V}^T v\right) \tag{9}$$

$$\{ui; vi\} = \arg \max_{u^T u=v^T v=1} u^T \delta_{uv}\, v, for\, i = 1, 2, 3, \ldots d\, a = 1 \tag{10}$$

Finally, these pairs are combined into a single matrix, yielding a fused resulting feature vector $X_3 \times K$denoted by $F_v(j)$. Subsequently, this vector is used to locate the tumor.

3.3. Proposal generation and refinement

After obtaining the fused features vector, the next critical objective is to formulate high-quality, class-independent, and fewer image proposals (regions or patches) in the feature map containing the tumor. A small number of proposals can improve object classification performance dramatically [24,25]. However, conventional approaches are insufficient to generate fewer yet higher-quality proposals. We first segmented the enhanced brain MRI images (feature map) to produce the initial set of locations. With segmentation, detection performance improves. It is preferred to use region-based over pixel-based segmentation since it conveys more information. First, the similarities between neighboring regions are evaluated, and the most similar neighbors are combined to form one region. The similarities between the two previously connected adjacent regions are assessed once more, and similar regions are united into one region. They were iteratively grouping comparable regions until all similar regions were consolidated into a single region to obtain an image.

Tumors may appear in the image at any scale. It is computationally impractical to exhaustively search for every possible location in the MRI image. A uniform grid, fixed scales, and fixed aspect ratios must be used to constrain the search space. The majority of the time, the number of locations to visit remains vast, where alternate limits must be enforced. Some tumors have fewer defined borders than others. Therefore, we must take into account all tumor scales. Due to the hierarchical nature of the grouping process, we may naturally generate locations at various scales by repeating the procedure until the entire image becomes a single region. This satisfies the criterion that all scales be captured. Whenever possible, we want to use region-based features because they can convey more information than pixels. Compared to an exhaustive search, fewer locations enable more advanced machine learning algorithms and computationally efficient tumor detection and classification models [23].

We aim to achieve a large number of proposals. At the moment, our proposals are based on the regions created due to grouping. Following receipt of the proposals, the next stage is to score and rank them. To do this, the structural edge detector will be used to extract the source image's edges. Compared to other edge detectors, this one is relatively fast and accurate. The edges are then connected according to their similarity in orientation to nearby edges. Edge groups are constructed by joining eight adjacent edges with an orientation difference greater than pi/2. Then, the affinities between them are computed using the mean locations and orientations of neighboring groupings. Only affiliations with values greater than 0.05 are retained; the remainder is discarded.

We calculated the score for our proposals based on these edge groups and their affinities. For each group, a continuous value $w_b(S_i)$ is computed to determine whether or not the specific set of edges S_i is contained inside the candidate bounding box$b$. If it is not totally contained inside the box b then $w_b(S_i) = 0$, the following mathematical procedure is used to decide which set of edges is entirely encased within the candidate bounding box$b$.

$$w_b = (S_i) = 1 - \max_t \prod_j^{|T|-1} a\left(t_j - t_j + 1\right) \tag{11}$$

Where t denotes the ordered path of edge groups, has a length of $|T|$, begins $t_1 \in S_b$ and ends at $t_{|T|} = S_i$, the continuous value $w_b(S_i)$ is set to 1 if Tdoes not exist, and a denotes the affinity between two edge groups.

The score function can be stated as follows using the values from Eq. (11).

$$\frac{\sum_i w_b(S_i)m_i}{2(b_w + b_h)^k} \tag{12}$$

Where b_w represents the box's width, b_h denotes the box's height, and $k$signifies the box's bias value for larger boxes. Finally, the generated proposals are prioritized using Eq. (12) and sent to our network for tumour classification. Fig. 4 illustrates the proposals generated.

3.4. Proposals alignment

The network's FC layers require fixed-size input to perform successive tasks, which is one of the primary issues when achieving object classification. Since the proposals generated will vary in size and shape. As a result, all developed proposals must be transformed to a specific size or shape. Region of interest (ROI) pooling generates proposals with defined measures. After obtaining the refined proposal or locations, a proposal alignment layer is applied to accomplish ROI pooling, resulting in a fixed-length feature vector of dimension 7×7. The output size of the ROI pooling does not depend on the number of proposals or the input feature map but rather on the number of sections whose number is equal to the output's dimension into which proposals should be divided. The primary benefit of adopting ROI pooling is that it speeds up processing, and the same input feature can be utilized for all generated proposals. This also improves the overall classification accuracy significantly. These proposals are shared across the remainder of our network to accomplish the needed objectives.

3.5. Classification

A new layer called mean pooling is introduced for the detection task, reducing the dimension of the feature map to one. After that, the final product will be generated by adding an FC layer of size$1 \times 1 \times 4$. The feature map obtained from the alignment layer is of poor resolution, three deconvolutional layers of size 3×3 are added to the output, followed by one convolutional layer. Following that, we apply the sigmoid function to our output to obtain three probability maps M_M,M_G,M_P. This is because the addition of three deconvolution layers improves the resolution of the preceding stage's proposals. The deconvolutional feature maps can be transmitted to the classification network to improve overall performance. The feature map we obtained for the classification layer is $1 \times 1 \times 1152$ pixels in size. This 1152 feature channels size is derived from 1024 feature channels derived from the backbone network and 128 feature channels derived from the deconvolution output. As illustrated in Fig. 2, this combination of features from two sources considerably improves classification performance. The likelihood p of each output class u is computed using the SoftMax activation function, which is defined as,

$$L_{classificaiton}(p, u) = -\log(p_u) \tag{13}$$

4. Evaluation and results

Dataset: The proposed model's efficiency was assessed using the public brain tumor dataset published by Cheng et al. [8], which can be found at (https://figshare.com/articles/braintumordataset/1512427). The data was gathered from 233 patients treated at two different state-owned hospitals in Guangzhou and Tianjin, China, between 2005 and 2010. It consists of 3064 T1-weighted enhanced contrast brain MRI scans with a resolution of 512×512pixels per image and a voxel spacing of$0.49 \times 0.49mm^2$. This dataset contains three distinct types of brain tumors, namely Pituitary, Meningioma, and Glioma, in three various planes, including axial, coronal, and sagittal views. The collection contains 930, 708, and 1426 occurrences of Pituitary, Meningioma, and Glioma cancers, respectively. The dataset is given in the matrix laboratory (MATLAB) format (.mat), which comprises a thorough description and a tumor mask, a

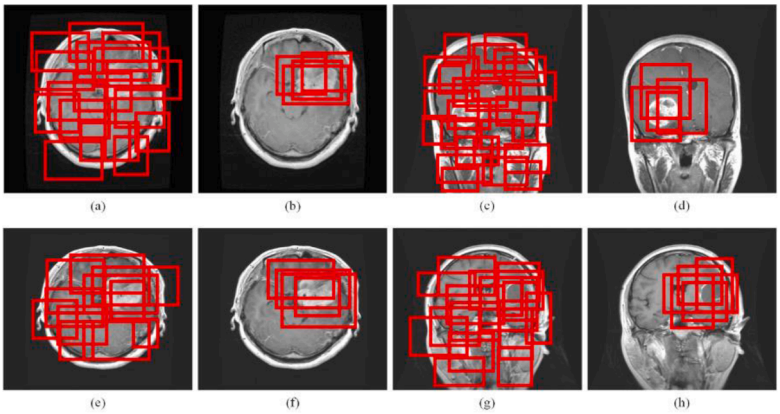

Fig. 4. High-quality tumor locations or proposals on several images.

tumor class label, a tumor border, and a patient ID. Generally, input images are brightened and recovered before further processing [19,21]. The images in this scenario were obtained utilizing a variety of imaging modalities, resulting in artifacts and inaccurate intensity levels. MRI images must be cleaned and enhanced for contrast. The main goal is to increase the dynamic range of grey values in images to improve visual quality. Fig. 4 shows three forms of brain tumors from sample pre-processed images. The primary objective is to expand the dynamic range of gray values in images to get a greater level of visual quality. Table 1 describes the dataset in detail, and representative pre-processed images exhibit three distinct types of brain tumors, as illustrated in Fig. 5.

Pre-processing and data augmentation: This step aids in enhancing and improving input data for the following task. We provided our network with an input brain MRI image to execute the desired classification task. Three views of each patient's MRI images were supplied to the network independently. A convolutional kernel is used to process the pixels' intensity in the input image. The convolutional kernel's performance is highly dependent on these intensity values in the MRI images. Since the pixel intensity values do not have a fixed meaning because they vary within and across subjects.

Moreover, the acquisition condition affects the intensity of image pixels. Numerous approaches and methodologies, most notably deep neural networks, are required to normalize the pixel intensity values in the input brain MRI image before performing any network optimization operation. The normalization technique can aid in acquiring almost identical intensity values for the provided source images, ensuring that the network converges robustly and consistently. The input MRI images are normalized using the min-max method in this research. Scaling the input image intensity values to a range between 0 and 1 significantly speeds up the network's training process. Another phase is contrast enhancement, which is necessary since MRI images are taken in various circumstances, settings, and modalities. False intensity levels and artifacts are a certainty in images, lowering their visual quality. As a result, image contrast and visual quality are boosted; additional details are provided in Section 3.1. The qualitative enhancement results for several images are shown in Fig. 6.

Data augmentation techniques increase the dataset sample size during the network training phase to reduce overfitting. Several versions of images are created using data augmentation techniques such as rotations and flipping. The objective is to expand the training dataset, and throughout the training process, images were rotated to different angles, notably 270°, 180°, and 90°. Images were also mirrored horizontally and vertically via a filliping technique to create visuals in both dimensions. As a result, the dataset is tripled in size in our scenario, yielding 9192 sample images. Fig. 7 illustrates the outcome of data augmentation.

Competitors: To determine the robustness and efficacy of the proposed brain tumor classification approach, the accuracy performance was compared to state-of-the-art mainstream methodologies [8,21]. The experimental findings demonstrate the effectiveness of the recommended technique.

Evaluation Matrix: The proposed model's performance was tested and confirmed; the accuracy of the system, specificity, sensitivity, precision, and f1-score were determined by quantifying the predicted classes with the following quantities: number of true-positive (TPN), number of true-negative (TNN), number of false-positive (FPN), and number of false-negative (FNN). Each matrix's mathematical representation is defined as follows:

$$accuracy = \frac{TP_N + TN_N}{TP_N + TN_N + FP_N + FN_N} \tag{14}$$

$$specificity = \frac{TN_N}{TN_N + FP_N} \tag{15}$$

$$sensitivity\, or\, recall = \frac{TP_N}{TP_N + FN_N} \tag{16}$$

$$precison = \frac{TP_N}{TP_N + FP_N} \tag{17}$$

$$f_1 - score = 2 \times \frac{recall \times precision}{recall \times precision} \tag{18}$$

Table 1
Description of the dataset used in the performance evaluation of the proposed model.

Tumor's categories	Number of patients involved in each category	Number of MRI images	Different planes/views of MRI Images
Glioma	89	1426	Coronal: 437 Sagittal: 495 Transverse (axial): 494
Meningioma	82	708	Coronal: 268 Sagittal: 231 Transverse (axial): 209
Pituitary	62	930	Coronal: 319 Sagittal: 320 Transverse (axial): 291
Overall	233	3064	Coronal: 1024 Sagittal: 1046 Transverse (axial): 994

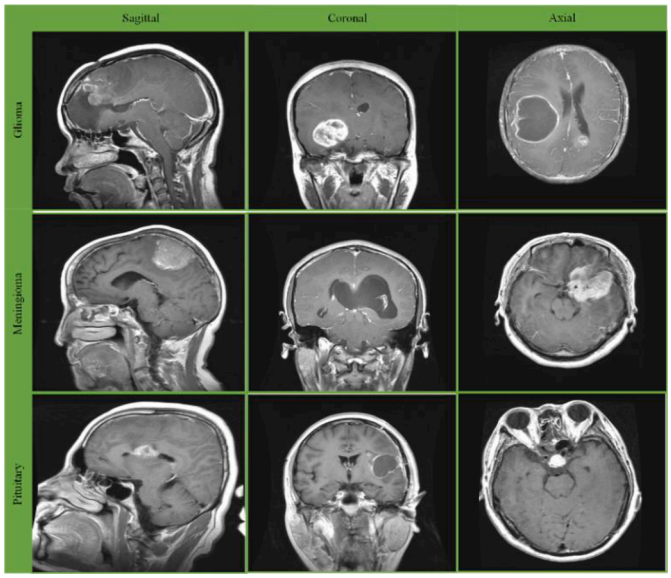

Fig. 5. Three distinct subtypes of brain tumors.

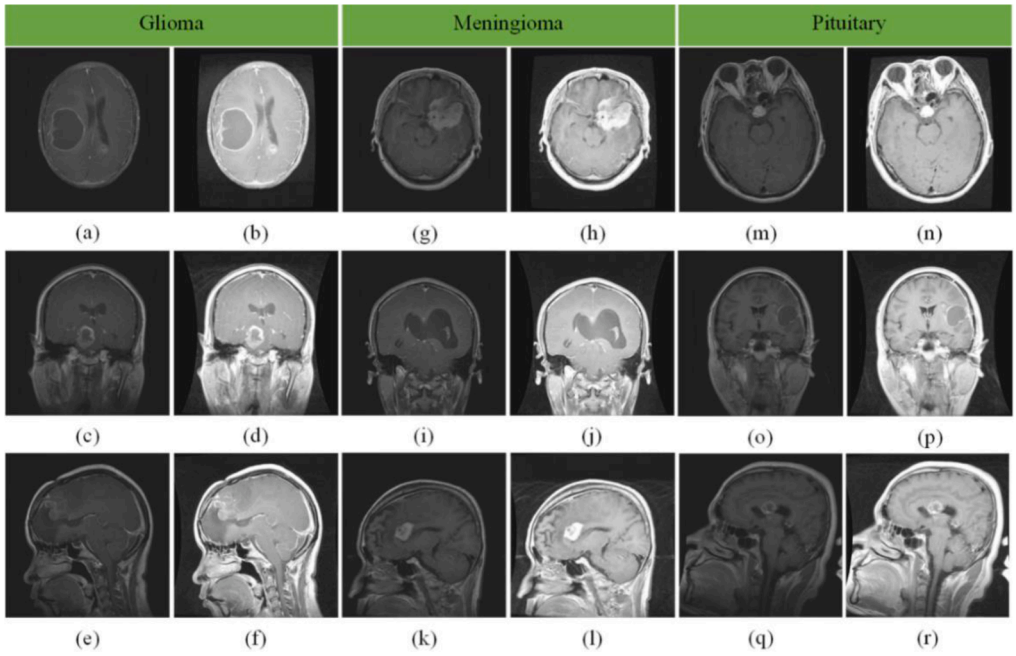

Fig. 6. The impact of quality enhancement on numerous images.

Hyper-parameters: Pre-processing involves normalizing and enhancing the input images to increase their quality. Using data augmentation approaches, the training process has been improved. The 5-fold cross-validation classification model is utilized to ensure adequate and comparable findings. The dataset is divided into two proportions: 70% for training and 30% for validation. Each experiment is performed five times, and the average is calculated to confirm the consistency of the results. Several experiments on training data were undertaken to assure the optimal selection of hyper-parameters for the final model assessment; the results are provided in Tables 2, 3, 4. When the learning rate was set to 0.003, the number of epochs to 20, the dropout to 0.5, and the batch size to 16, the suggested model attained a high level of accuracy for the Adgrade optimizer. We used Cheng et al. 5-fold cross-validation to assess the performance of the proposed model [8]. This method is more consistent in producing valid and distinct classification results.

Tables 6 and 7 show the final findings. Over-fitting was significantly decreased, and the proposed model converged faster. It offers a high retrieval accuracy while consuming little processing power. The model is straightforward to deploy, and radiologists might favor

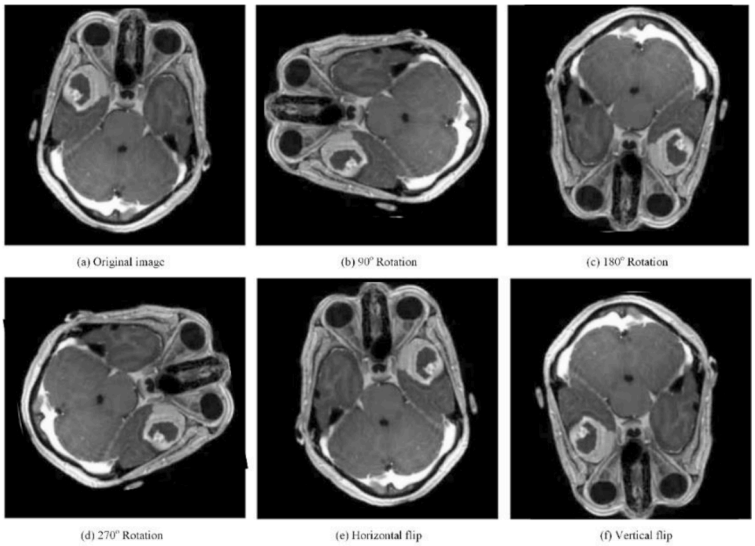

Fig. 7. Numerous image variants were generated using data augmentation techniques.

Table 2
The proposed method's accuracy assessment based on different learning rates using various optimization algorithms.

Optimizer	Learning Rate					
	0.1	**0.01**	**0.001**	**0.002**	**0.003**	**0.004**
Adam	68.91	73.10	81.78	81.45	84.26	78.71
SGD	87.82	**93.61**	89.22	91.77	91.05	92.42
Adadelta	**89.01**	85.96	79.30	82.17	83.68	83.94
RMSprop	82.78	84.96	80.51	81.16	83.46	81.11
Adagrad	84.88	92.84	**97.09**	**97.32**	**98.95**	**96.57**

Table 3
Comparison of the proposed model's average accuracy on different epoch numbers.

Number of Epochs	10	20	30	40
Overall accuracy	98.74	**98.95**	98.72	98.83

it for decision-making classification tasks. The proposed method is a robust design that is more applicable to the objective of brain classification.

5. Experimental results

A confusion matrix based on the model's correct and incorrect predictions is developed to evaluate the proposed system's performance. The confusion matrix obtained throughout the experiments is shown in Table 5. As can be seen, the proposed model properly classified 3009 examples and wrongly classified 55 cases, yielding an overall accuracy of 98.95%. It is worth noting that Glioma had the greatest prediction proportion. This finding is attributable to the larger training dataset gained through various augmentation approaches. The dataset's balance considerably improved the classification results. The classifier's performance was evaluated using this confusion matrix in terms of accuracy, sensitivity (recall), specificity, and f1-score for each tumor type. Table 6 demonstrates how well the proposed classifier worked for each type of brain tumor. For Meningioma, Glioma, and Pituitary classes, the proposed model has an accuracy of 98.30%, 98.72%, and 99.37%, sensitivity (recall) of 97.31%, 97.83%, and 99.46%, and specificity of 98.59%, 99.51%, and 99.34%, respectively. The model also achieved high precision values of 95.42%, 99.43%, and 98.50%, and f_1-score values of 96.35%, 98.62%, and 98.97% for three classes, indicating that our technique is more suited for classifying brain cancers from MRI scans.

Table 4
Comparison of the proposed model's average accuracy on different dropout rates.

Dropout rates	0.1	0.3	0.5	0.7
Overall accuracy	98.64	98.89	**98.95**	98.12

Table 5
Summary of the proposed model's prediction results on brain tumor classification problem.

Predicted Values				
Actual Values	Class	Meningioma	Glioma	Pituitary
	Meningioma	689	8	11
	Glioma	28	1399	3
	Pituitary	5	0	921

This is undeniably due to our model's high efficiency in classifying tumors in sample images. It is worthy to note that the proposed method acquired high specificity values for all classes, implying that it accurately diagnoses sample images that do not include the specific disease. Compared to other methods, our method's efficiency and performance were superior. By increasing the number of sample images, the model's efficiency is enhanced while also addressing the issue of over-fitting. The proposed method avoided manual segmentation and did not require prior knowledge of the feature types to retrieve, limiting the network's generalizability [14]. We conclude that our model has a reasonable degree of generalization and retains its stability.

The proposed technique applies to various applications, including the classification of breast tumors. The proposed method is compared to other well-known algorithms for classifying three-class brain tumors using the same dataset as in Table 7. This table summarizes the classification performance based on the accuracy metric utilized in all earlier techniques. As indicated in Tables 2, 3, and 4, the proposed model is evaluated on various factors to ensure robust performance. The proposed method achieved the highest accuracy of 98.95% in only 20 epochs without manual segmentation compared to others. This accuracy demonstrates the effectiveness of the proposed strategy for feature extraction and classification of brain tumors using deep learning. Additionally, the proposed method outperformed competitors not only in terms of accuracy but also in terms of overall performance across every quality criterion.

Fig. 8 illustrates the proposed model's classification performance receiver operating characteristic (ROC) curve. The proposed model generates outstanding results, with correlation coefficients of 0.9859, 0.9951, and 0.9934 for the Meningioma, Glioma, and Pituitary classes. Glioma had the highest valid positive rate compared to other tumor types. Fig. 9 illustrates the proposed method's detection efficiency compared to alternative methods for object detection [24,25]. The average accuracy curve in Fig. 9 demonstrates the usefulness of the proposed method's detection efficiency. It shows a performance comparison of detection rate (recall) versus IoU overlap threshold. When employed only 100 proposals per image, we achieved the maximum detection recall of 95.4%. It demonstrates that the method of drawing a bounding box to detect the tumor is stable. Experiments indicated that optimizing hyper-parameters and constructing an appropriate architecture improved performance, putting it ahead of the competition. The classification of brain tumors is a complex problem. Numerous factors can affect the classification process, including tumor shape, orientation, and size, low contrast in MRI images, and a scarcity of training samples. This can lead to overfitting and misclassification, lowering classification accuracy.

In comparison to previous approaches, the proposed methodology tackles these issues significantly while retaining an acceptable level of accuracy. Before performing classification tasks, tumor localization, contrast enhancement, and data augmentation contribute to the proposed method's increased classification accuracy, distinguishing it from others. Thus, the model achieved good classification results, promptly reached its peak performance, and significantly reduced the problem of over-fitting. Fig. 10 and Fig. 11 illustrate the network's training and validation phases. The accuracy and loss curves indicate that the model performed admirably and maintained a high consistency throughout the training and validation stages.

6. Conclusions

Brain tumor classification is a critical subject of medical research. The study proposes a method for accurately and simply classifying brain tumors, including Meningiomas, Gliomas, and Pituitaries, using brain MRI data. Optimal contrast and non-linear techniques are used to enhance image quality. By using segmentation and clustering, tumor locations are determined. These scored locations are sent to EfficientNet-B0 for feature extraction with the associated input image. To improve detection performance, these locations are further fine-tuned. Then, these locations are aligned and analyzed to identify the tumor category and location. By shifting

Table 6
The performance valuation of the proposed method on different quality measures.

Tumor type	Accuracy	Sensitivity (Recall)	Specificity	Precision	f_1-score
Meningioma	98.30	97.31	98.59	95.42	96.35
Glioma	98.72	97.83	99.51	99.43	98.62
Pituitary	99.37	99.46	99.34	98.50	98.97

Table 7
Comparison of the proposed model with other existing approaches.

Refs.	Approaches	Extracted Features	Manual segmentation	Number of images used	Overall accuracy %	Assessment Method
[8]	BoW-SVM	BOW	Yes	3064	91.28	Introduced split
[9]	NN	DWT-Gabor	Yes	3064	91.9	Training -validation
[10]	Preprocessing-SVM	2D DWT using Daubechies wavelets base	No	3064	86	10-fold cross-validation (split)
[11]	ConvNet $^{64 \times 64}$	CNN	No	989 (axial only)	84.52	5-fold cross-validation (split)
[11]	ConvNet 256×256	CNN	No	989 (axial only)	90.26	5-fold cross-validation (split)
[12]	CapsNet	CNN	Both	3064	86.56 using segmentation 72.13 using raw images	Not mentioned
[13]	CapsNet	CNN	Bounding box	3064	90.89	Not mentioned
[14]	Holistic-RNN (LSTM-Autoencoder)	Dense CNN	No	989(axial only)	92.13	Training-validation testing
[15]	ELM	CNN	Not mentioned	3064	93.68	Training-validation
[16]	Different ConvNet	Model based	No	2100 (700 from each tumor type)	84.19	Training-validation
[17]	GAN-ConvNet	CNN	No	3064	93.01	Introduced split
[17]	GAN-ConvNet	CNN	No	3064	95.6	5-fold cross-validation
[18]	GA + CNN	CNN	No	989 (axial only)	94.2	Training- Validation
[19]	CapsNet	CNN	No	3064	94.74	5-fold cross-validation
[20]	deep CNN-SVM	CNN	No	3064	97.1	5-fold cross-validation
[21]	EfficientNet-B0	CNN	Bounding Box	3064	98. 04	5-fold cross-validation
Our's method	EfficientNet-B0,ResNet50	CNN	Bounding Box	3064	98.95	5-fold cross-validation

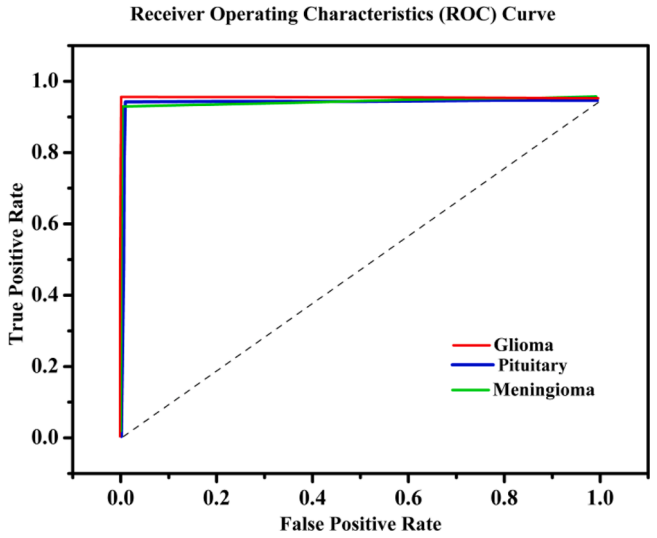

Fig. 8. The ROC curve for the proposed approach.

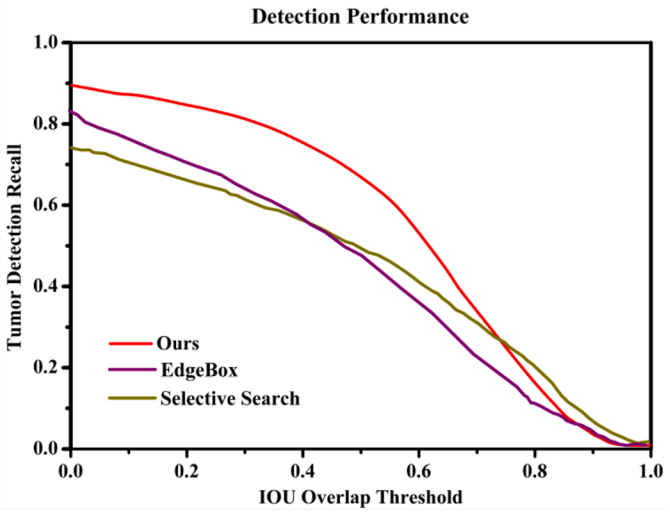

Fig. 9. The detection rate (recall) was compared against the IoU overlap threshold using 100 proposals per image.

features from detection to classification layers, classification accuracy was improved. In addition, data augmentation techniques were applied to avoid network overfitting. An evaluation of the proposed model was performed using the free FigShare dataset. Compared to other approaches of a similar type, the experiments provided robust results. Overall, the proposed technique achieved 95.98% classification accuracy. For the Meningioma, Glioma, and Pituitary classes, our model achieved greater accuracy (98.31%, 98.72%, 99.46%), sensitivity (97.31%, 97.83%, and 99.46%), and specificity (98.59%, 99.51%, and 99.34%). Hence, the porposed model appears to be effective for classifying brain tumors.

Since the proposed model's classification accuracy is proportional to the number of training images, a small dataset would reduce its performance. An extensive dataset, however, can also be computationally expensive. By reducing the computational cost of the proposed model, it can also be used in breast tumor classification and liver lesion classification when CT, PET, and X-ray images are employed. A weakly supervised learning method may increase tumor localization accuracy. Moreover, multichannel classifiers will enhance the model's performance. Callback functions on minimal loss and maximum accuracy can be introduced for determining the number of epochs.

Declaration of Competing Interest

Conflict of Interest and Authorship Conformation Form Please check the following as appropriate: o All authors have participated in (a) conception and design, or analysis and interpretation of the data; (b) drafting the article or revising it critically for important

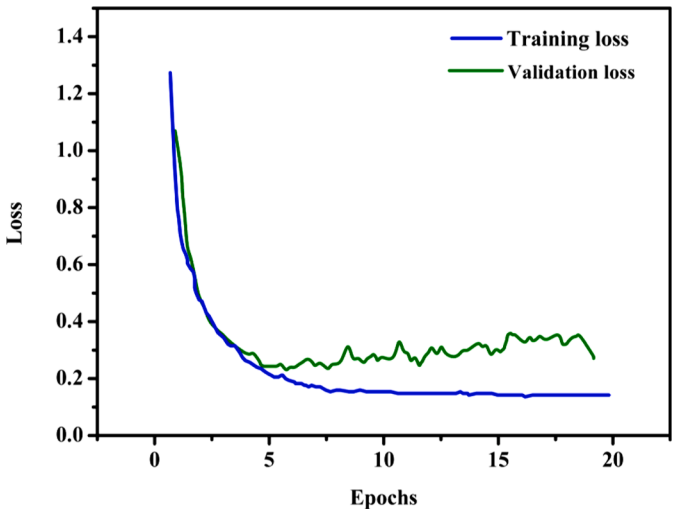

Fig. 10. The proposed method's loss trend.

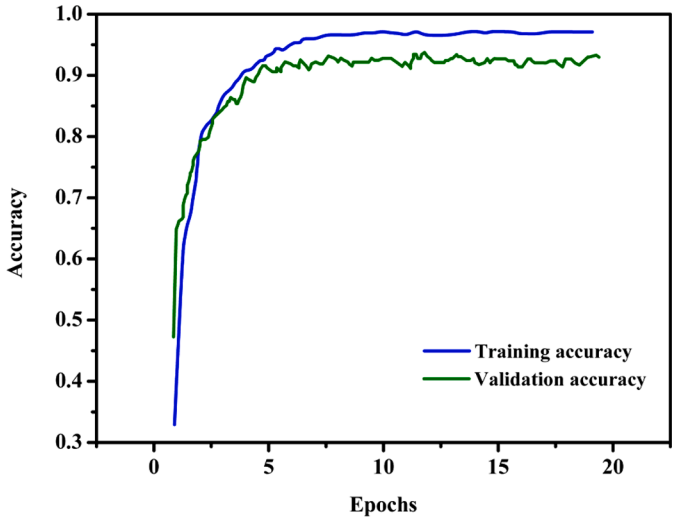

Fig. 11. The proposed method's accuracy trend.

intellectual content; and (c) approval of the final version. o This manuscript has not been submitted to, nor is under review at, another journal or other publishing venue. o The authors have no affiliation with any organization with a direct or indirect financial interest in the subject matter discussed in the manuscript.

Acknowledgment

This research work is supported by The University Research Innovation Fund of Science and Technology Development Center of the Ministry of Education of China (2020ITA05022), The Natural Science Foundation of Hubei Province (2021CFB316), The Preliminary Support Project of Hubei Social Science Foundation (21ZD137), The Hundreds of Schools Unite with Hundreds of Counties-University Serving Rural Revitalization Science and Technology Support Action Plan (BXLBX0847).

References

[1] Yu K, Tan L, Lin L, Cheng X, Yi Z, Sato T. Deep-learning-empowered breast cancer auxiliary diagnosis for 5GB remote E-health, 28. IEEE Wirel Commun; 2021 Jul 19. p. 54–61.
[2] Masood M, Nazir T, Nawaz M, Mehmood A, Rashid J, Kwon HY, Mahmood T, Hussain A. A novel deep learning method for recognition and classification of brain tumors from MRI images. Diagnostics 2021;11(5):744. May.
[3] Irmak E. Multi-classification of brain tumor MRI images using deep convolutional neural network with fully optimized framework. Iran J Sci Technol 2021;45 (3):1015–36. Sep Transactions of Electrical Engineering.

[4] Nawaz M, Nazir T, Masood M, Mehmood A, Mahum R, Khan MA, Kadry S, Thinnukool O. Analysis of brain MRI images using improved CornerNet approach. Diagnostics 2021;11(10):1856. Oct.
[5] Sharif MI, Khan MA, Alhussein M, Aurangzeb K, Raza M. A decision support system for multimodal brain tumor classification using deep learning. Complex Intell Syst 2021 Mar 9:1–4.
[6] Abd-El Kader I, Xu G, Shuai Z, Saminu S, Javaid I. Salim Ahmad I. Differential deep convolutional neural network model for brain tumor classification. Brain Sci 2021;11(3):352. Mar.
[7] Singh R, Goel A, Raghuvanshi DK. Computer-aided diagnostic network for brain tumor classification employing modulated Gabor filter banks. Vis Comput 2021; 37(8):2157–71.
[8] Cheng J, Huang W, Cao S, Yang R, Yang W, Yun Z, Wang Z, Feng Q. Enhanced performance of brain tumor classification via tumor region augmentation and partition. PloS one 2015 Oct 8;10(10):e0140381.
[9] Ismael MR, Abdel-Qader I. Brain tumor classification via statistical features and back-propagation neural network. In: 2018 IEEE International Conference on Electro/Information Technology (EIT); 2018 May 3. p. 0252–7.
[10] Tahir B, Iqbal S, Usman.Ghani. Khan M, Saba T, Mehmood Z, Anjum A, Mahmood T. Feature enhancement framework for brain tumor segmentation and classification. Microsc Res Tech. 2019 Jun;82(6):803-11.
[11] Paul JS, Plassard AJ, Landman BA, Fabbri D. Deep learning for brain tumor classification. Medical Imaging 2017: Biomedical Applications in Molecular, Structural, and Functional Imaging 2017 Mar 13;10137:1013710.
[12] Afshar P, Mohammadi A, Plataniotis KN. Brain tumor type classification via capsule networks. In: 2018 25th IEEE International Conference on Image Processing (ICIP); 2018 Oct 7. p. 3129–33.
[13] Afshar P, Plataniotis KN, Mohammadi A. Capsule networks for brain tumor classification based on MRI images and coarse tumor boundaries. In: InICASSP 2019-2019 IEEE International Conference on Acoustics, Speech and Signal Processing (ICASSP); 2019 May 12. p. 1368–72.
[14] Zhou Y, Li Z, Zhu H, Chen C, Gao M, Xu K, Xu J. Holistic brain tumor screening and classification based on DenseNet and recurrent neural network. In International MICCAI Brainlesion Workshop 2018 Sep 16:208–17.
[15] Pashaei A, Sajedi H, Jazayeri N. Brain tumor classification via convolutional neural network and extreme learning machines. In: 2018 8th International conference on computer and knowledge engineering (ICCKE); 2018 Oct 25. p. 314–9.
[16] Abiwinanda N, Hanif M, Hesaputra ST, Handayani A, Mengko TR. Brain tumor classification using convolutional neural network. World congress on medical physics and biomedical engineering 2018;2019:183–9.
[17] Ghassemi N, Shoeibi A, Rouhani M. Deep neural network with generative adversarial networks pre-training for brain tumor classification based on MR images. Biomed Signal Process Control 2020 Mar 1;57:101678.
[18] Anaraki AK, Ayati M, Kazemi F. Magnetic resonance imaging-based brain tumor grades classification and grading via convolutional neural networks and genetic algorithms. Biocybern Biomed Eng 2019 Jan 1;39(1):63–74.
[19] Ayadi W, Elhamzi W, Charfi I, Atri M. Deep CNN for brain tumor classification. Neural Process Lett 2021;53(1):671–700.
[20] Deepak S, Ameer PM. Brain tumor classification using deep CNN features via transfer learning. Comput Biol Med 2019 Aug 1;111:103345.
[21] Guan Y, Aamir M, Rahman Z, Ali A, Abro WA, Dayo ZA, et al. A framework for efficient brain tumor classification using MRI images. Math Biosci Eng 2021 Jun 1;18(5):5790–815.
[22] Al-Ameen Z. Nighttime image enhancement using a new illumination boost algorithm. IET Image Proc 2019 Jun 20;13(8):1314–20.
[23] Khan MA, Ashraf I, Alhaisoni M, Damaševičius R, Scherer R, Rehman A, Bukhari SA. Multimodal brain tumor classification using deep learning and robust feature selection: A machine learning application for radiologists. Diagnostics 2020 Aug; 10;(8):565.
[24] Uijlings JR, Van De Sande KE, Gevers T, Smeulders AW. Selective search for object recognition. Int J Comput Vis 2013 Sep; 104;(2):154–71.
[25] Zitnick CL, Dollár P. Edge boxes: Locating object proposals from edges. In: European conference on computer vision; 2014 Sep 6. p. 391–405.

Muhammad Aamir is an Associate Professor in the Department of Computer Science at Huanggang Normal University, China. He has several years of research experience and has been widely published. His research spans multiple areas, including pattern recognition, computer vision, image processing, deep learning, fractional calculus, and organization behavior.

Ziaur Rahman obtained the Ph.D. degree from Sichuan University, China, in 2020. Currently, he is working as an Associate Professor at the Department of Computer Science, Huanggang Normal University, China. His research interests include image processing, computer vision, deep learning, and fractional calculus.

Zaheer Ahmed Dayo (Member, IEEE) is currently associated with the College of Computer Science, Huanggang Normal University, China, as an Associate Professor. He earned the Ph.D. degree in Communication Information Systems from the College of Electronics and Information Engineering, Nanjing University of Aeronautics & Astronautics, China. His core research focused towards the RF and microwave engineering, IoT and deep learning. .

Waheed Ahmed Abro is currently pursuing a doctorate at Southeast University, Nanjing, China. His research interests include natural language processing, spoken language understanding, computer vision, and pattern recognition.

M. Irfan Uddin is currently working at the Institute of Computing, Kohat University of Science and Technology, Kohat, Pakistan. He received Ph.D. in Computer Science. He worked as a postdoctoral researcher in EU funded project. His research interest includes; machine learning, data science, artificial neural networks, deep learning, computer vision, machine translation, natural language processing, speech recognition, big data analytics, and parallel programming/Multi H core/Many-core/GPUs.

Inayat Khan received the Ph.D. degree in Computer Science from the Department of Computer Science, University of Peshawar, Pakistan. His current research is based on the design and development of context-aware adaptive user interfaces for minimizing drivers' distractions. His other research interests include lifelogging ubiquitous computing, and he has published several articles in international journals and conferences in these areas.

Ali Shariq Imran (Member, IEEE) is currently associated with the Department of Computer Science, Norwegian University of Science and Technology (NTNU), Norway, as an Associate Professor. He is a member of Norwegian Colour and Visual Computing Laboratory (Colourlab) and an IEEE Member, Norway Section. He is also an Associate Editor to open access journals, including IEEE Access, and has served as a guest editor for Elsevier and Springer journals.

Zafar Ali received his Ph.D. degree in Computer Science and Technology (2021) from the School of Computer Science and Engineering, Nanjing, China. His research interests include information retrieval, recommendation systems, deep learning, NLP, and the semantic web. He has published papers in international venues, namely AI Review, Knowledge-based systems, ESWA, NCAA, Neurocomputing, and IJCNN.

Muhammad Ishfaq is an Associate Professor associated with Department of Computer Science, Huanggang Normal University. His research interests include pharmacology, toxicology, artificial intelligence, machine learning, signaling pathways, in-silico methods, immunology, infectious diseases, modelling, etc.

Yurong Guan graduated from Wuhan University of Technology in China with a Master of Social Computer Application degree in 2008. She is currently working on her doctorate at the Central University of the Philippines. She is a Professor and master's degree supervisor at Huanggang Normal University's Department of Computer Science. Her research interests include digital image processing and Java software development.

Zhihua Hu has obtained the doctoral degree from Wuhan University, currently working as a Professor and a master's degree Supervisor at Huanggang Normal University, China. He held several local research projects and published more than 50 papers in reputed international journals. His research interests include digital image processing and information security.